Distinct pH dependencies of Na^+/K^+ selectivity at the two faces of Na,K-ATPase

Received for publication, October 30, 2017, and in revised form, November 28, 2017 Published, Papers in Press, December 15, 2017, DOI 10.1074/jbc.RA117.000700

Flemming Cornelius[‡1], **Naoki Tsunekawa**[§], **and Chikashi Toyoshima**[§]

From the [‡]*Department of Biomedicine, University of Aarhus, Ole Worms Allé 6, 8000 Aarhus C, Denmark and the* [§]*Institute of Molecular and Cellular Biosciences, University of Tokyo, Bunkyo-ku, Tokyo 113–0032*

Edited by Roger J. Colbran

The sodium pump (Na,K-ATPase) in animal cells is vital for actively maintaining ATP hydrolysis–powered Na^+ and K^+ electrochemical gradients across the cell membrane. These ion gradients drive co- and countertransport and are critical for establishing the membrane potential. It has been an enigma how Na,K-ATPase discriminates between Na^+ and K^+, despite the pumped ion on each side being at a lower concentration than the other ion. Recent crystal structures of analogs of the intermediate conformations E2·Pi·2K^+ and Na^+-bound E1∼P·ADP suggest that the dimensions of the respective binding sites in Na,K-ATPase are crucial in determining its selectivity. Here, we found that the selectivity at each membrane face is pH-dependent and that this dependence is unique for each face. Most notable was a strong increase in the specific affinity for K^+ at the extracellular face (*i.e.* E2 conformation) as the pH is lowered from 7.5 to 5. We also observed a smaller increase in affinity for K^+ on the cytoplasmic side (E1 conformation), which reduced the selectivity for Na^+. Theoretical analysis of the pK_a values of ion-coordinating acidic amino acid residues suggested that the face-specific pH dependences and Na^+/K^+ selectivities may arise from the protonation or ionization of key residues. The increase in K^+ selectivity at low pH on the cytoplasmic face, for instance, appeared to be associated with Asp^{808} protonation. We conclude that changes in the ionization state of coordinating residues in Na,K-ATPase could contribute to altering face-specific ion selectivity.

Under physiological conditions Na,K-ATPase actively extrudes three cytoplasmic Na^+ ions in exchange for two extracellular K^+ ions by hydrolyzing one molecule of ATP. The established gradients for Na^+ and K^+, pivotal for generating membrane potential and regulating cell volume, also provide the chemical energy for secondary active transport of various substrates and ions (1). In the reaction cycle, the Na,K-ATPase changes between two main conformations: an E1 conformation, where the binding sites are inward-facing and exposed to the cytoplasm and preferentially bind Na^+; and an E2 conformation, where they are outward-facing and exposed to the extracellular side and preferentially bind K^+. At both membrane faces the Na^+/K^+ ion concentration ratios are unfavorable; at the cytoplasm-facing binding sites, the K^+ concentration is more than 10 times higher than the Na^+ concentration, and at the externally facing sites, the Na^+ concentration is about 30 times higher than the K^+ concentration. Moreover, the apparent affinities for Na^+ and K^+ are in the mM range. Nevertheless, the selectivity for Na^+ over K^+ at the cytoplasmic face is ∼10-fold, and at the extracellular side there is a K^+/Na^+ selectivity of more than 100-fold (2). Based on the crystal structure of the Na^+-bound E1∼P·ADP form, we recently hypothesized that the ion selectivity at the cytoplasmic face of the pump depends on size discrimination, where only the smaller Na^+ ions fit into the binding sites (3).

pH has been demonstrated previously to have a significant impact on Na,K-ATPase apparent ion affinities and activity (4–6), which has been ascribed mainly to an effect on the E1/E2 equilibrium distribution (7, 8). In the closely related SERCA1a, however, protonation of acidic residues is structurally important (9, 10), leading to improved ion–residue interactions (11, 12). Recent electrophysiological results using Na,K-ATPase expressed in *Xenopus* oocytes demonstrate that an increase in external pH results in external K^+ competing less well with external Na^+ (13), and molecular dynamics (MD)[2] simulations further suggest that differences in the protonation state of key acidic residues in the binding sites are important for ion selectivity (13–15).

In this study we examined how Na^+/K^+ selectivity and the ion affinities in the two main conformations E1 and E2 are affected by changes in pH. The two faces of the pump have different ion affinities and therefore can be functionally separated, and the Na^+/K^+ selectivity at both the extracellularly and intracellularly facing ion sites can be investigated. Moreover, pK_a estimations of key acidic residues were performed using continuum electrostatic calculations and PROPKA 3.1 with the detailed structure of the Na^+ and K^+-binding sites obtained from high-resolution crystal structures in the E1∼P·ADP·3Na^+ and the E2·Pi·2K^+ states (3, 16) (Fig. 1). It is suggested that the different apparent ion affinities and thus Na^+/K^+ selectivities observed at the two faces of the pump at varying pH are a result of changes in the detailed structure around the ions, possibly depending on the protonation state of critical binding residues, which differ at the extracellular and cytoplasm-facing sites.

This work was supported by grants from the Danish Medical Research Council, the Danish Agency for Science, Technology, and Innovation, and the Novo Nordisk Foundation. The authors declare that they have no conflicts of interests with the contents of this article.

[1] To whom correspondence should be addressed. Tel.: 45-87167746; E-mail: fc@biomed.au.dk.

[2] The abbreviations used are: MD, molecular dynamics; MCCE, multiconformation continuum electrostatic calculation.

Results

pH-dependence of Na,K-ATPase hydrolytic activity

Fig. 2*A* (□) shows the familiar bell-shaped pH dependence of Na,K-ATPase activity measured at three different K^+ concentrations. The distribution broadens as the K^+ concentration decreases, and the activity has an optimum that is slightly left-shifted to lower pH values at increasing K^+ concentrations. The bell-shaped curves are not caused by irreversible enzyme inactivation, which takes place only at a more extreme pH, as indicated by the activity measurements at optimal pH of 7.4 after preincubation at the test pH (Fig. 2*A*, ○). As observed, the enzyme activity is stable between pH 4.5 and up to about 9.5. Only outside this pH interval is irreversible inactivation observed. The irreversible inactivation is independent of K^+ concentration. The time dependence of enzyme inactivation at different pH values is shown in Fig. 2*B*. The first-order rate constants for inactivation are 0.70 min^{-1} at pH 4.0, 0.0021 min^{-1} at pH 9.5, and 0.059 min^{-1} at pH 10.2. The irreversible inactivation induced by very low and very high pH is associated with structural instability, as observed by increased trypsin sensitivity at these extreme pH values (Fig. 3). As seen from the 95-kDa band intensity in the immunoblot representing unsplit enzyme, the E1 conformation is slightly more trypsin-resistant than the E2 form at physiological pH 7.4. The reversible decrease in enzyme activity outside the pH optimum suggests the formation of suboptimal ionic forms of the enzyme. This could be accompanied by changes in the protonation state of ionizable residues in the cation-binding sites, as already suggested by Skou (7). One such residue could be Glu^{327} in the extracellularly facing K^+ sites, which is expected to become deprotonated at high pH values (Table 1) because its mutation to Gln, used as a substitute for protonated Glu, removes the inhibition at high pH (17).

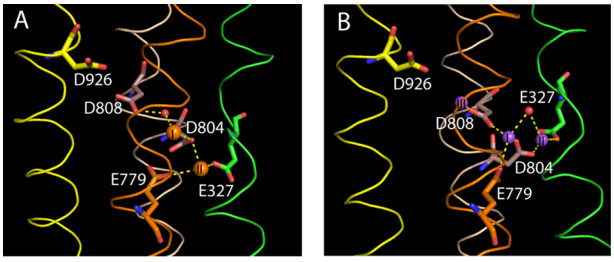

Figure 1. Coordinating residues in the K^+ (*A*)- and Na^+ (*B*)-binding sites viewed approximately parallel to the membrane. The M4 helix is *green*, M5 is *orange*, M6 is *wheat-colored*, and M8 is *yellow*. *Orange spheres* indicate K^+ ions and *violet spheres* Na^+ ions, and the *red sphere* is water.

Na^+/K^+ selectivity at the cytoplasmic face of the Na,K-ATPase

Scheme 1 illustrates K^+ competition for Na^+ at the inward-facing sites in the E1 enzyme form.

$$E1\cdot Na_3^+ \underset{k_{-Na}}{\overset{k_{Na}[Na]^3}{\rightleftharpoons}} E1 \underset{k_K[K]^3}{\overset{k_{-K}}{\rightleftharpoons}} E1\cdot K_3^+$$

Scheme 1

If K^+ is assumed to be a simple competitive inhibitor at the three cytoplasm-facing Na^+ sites, the Na^+ activation curves at different fixed K^+ concentrations can be analyzed using the Hill formalism given by Equation 1, derived from the steady-state solution of Scheme 1 (18–20),

$$v = \frac{V_{max}}{(1 + K'_{Na}/[Na^+_{cyt}])^{n_H}} \quad \text{(Eq. 1)}$$

where n_H is the Hill coefficient, which is smaller than the number of binding sites unless cooperativity is very high, and K'_{Na}, the intrinsic site dissociation constant for Na^+, is a linear function of the cytoplasmic K^+ concentration.

$$K'_{Na} = K^0_{Na} + \frac{K^0_{Na}}{K_K}[K^+_{cyt}] \quad \text{(Eq. 2)}$$

K^0_{Na} is the apparent dissociation constant for Na^+ in the absence of K^+, and K_K is the apparent dissociation constant for cytoplasmic K^+ as a competitive inhibitor. Therefore, the slope K^0_{Na}/K_K (or rather 1/slope, because the affinity and dissociation constants are inversely related) of the linear

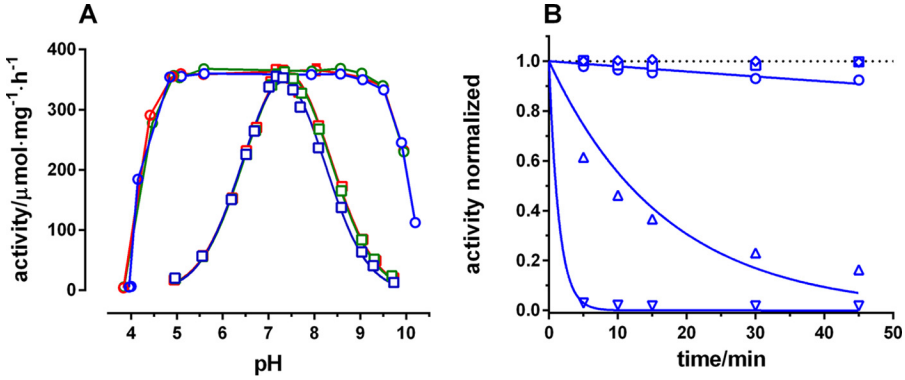

Figure 2. pH dependence of hydrolytic activity (23 °C) at three different K^+ concentration (5, 20, and 50 mM) with the sum of $[Na^+] + [K^+] = 150$ mM. Measurements are an average of three measurements with S.D. represented by the *error bars* (smaller here than the *symbols*). In *A*, the *square symbols* represent activity measured at the indicated pH. The pH optimum is 7.41 ± 0.010 for 5 mM K^+ (*green squares*), 7.41 ± 0.006 for 20 mM K^+ (*red squares*), and 7.32 ± 0.009 for 50 mM K^+ (*blue squares*). The stability of the enzyme at the various pH values was tested by preincubating the enzyme at the test pH for 15 min followed by measuring the activity at the pH optimum of 7.4 (*circles*). As indicated, the enzyme is completely stable at pH values between 5.0 and 9.5. Outside of this pH interval, irreversible inactivation occurs at all K^+ concentrations tested. *B*, the inactivation curves in the presence of 100 mM Na^+ and 50 mM K^+ at different pH values (▽, pH 4.0; □, pH 5.0; ◇, pH 7.2; ○, pH 9.5; △, pH 10.2). The enzyme was preincubated at the indicated pH for variable time periods, and the activity was then measured at pH 7.4. The curves are exponential fits to the data, with no constraints on the fit parameters. The first-order rate constants of inactivation are 0.70 ± 0.06 min^{-1} at pH 4.0, 0.0021 ± 0.002 min^{-1} at pH 9.5, and 0.059 ± 0.004 min^{-1} at pH 10.2.

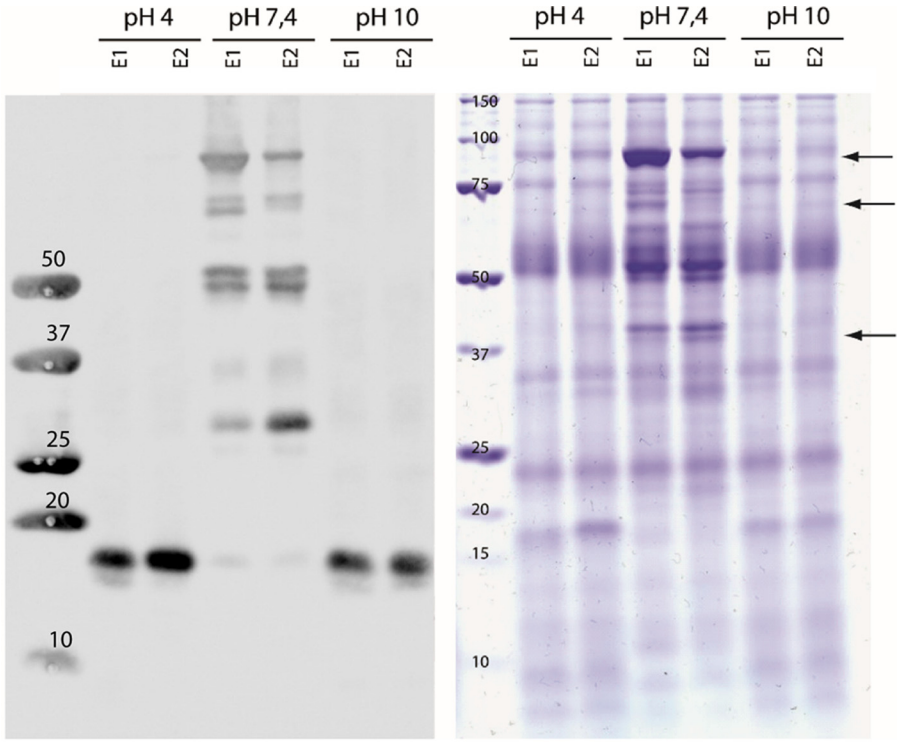

Figure 3. Trypsin fingerprint of enzyme incubated at pH 4, 7.4, and 10 in the presence of either 150 mM NaCl (E1) or 150 mM KCl (E2) followed by trypsin digestion at pH 7.4. *Right*, Coomassie-stained SDS gel. *Left*, immunoblot reacted with anti-α antibody raised to the C terminus. *Arrows* indicate variable band patterns in E1 and E2 at pH 7.4.

Table 1

pK_a values of K^+-and Na^+-binding site residues calculated using PROPKA or MCCE

Empirical pK_a values were calculated by the method PROPKA 3.1 or MCCE 2.7 with a dielectric constant of 4. *, indicates that the residues are strongly coupled in the E1 and E2 states; †, indicates that the residue is strongly coupled in the E1 state. Individual pK_a values calculated for these residues are interdependent and ambiguous. In the MCCE calculations for the E1 conformation all three residues were treated together as explained under "Experimental Procedures." Numbering is according to pig kidney.

Residue	E2		E1			
	2ZXE(A)		3WGV(A)		3WGV(C)	
	PROPKA	MCCE	PROPKA	MCCE	PROPKA	MCCE
Glu327*	8.2	12.8	10.7	1.8, 12.0, >14	11.1	1.1, 7.1, >14
Glu779*	10.4	>14	9.5		9.4	
Asp804*	3.2	<0	5.4		5.3	
Asp808†	5.8	2.6	3.1	<0	3.2	<0
Asp926	8.9	>14	6.3	0.5	6.5	<0
Glu954	10.3	>14	9.6	>14	9.7	>14

relationship of Equation 2 is a measure of the Na^+/K^+ selectivity. Note that K'_{Na}, the intrinsic site dissociation constant for Na^+, does not equal the half-saturation constant ($K_{0.5}$). Actually, $v = \frac{1}{2}V_{max}$ when $K_{0.5} = 3.8\,K'_{Na}$ in this model when assuming $n_H = 3$.

Fig. 4 shows the Na^+ activation of Na,K-ATPase measured at physiological pH 7.5 at different fixed K^+ concentrations between 5 and 50 mM, *i.e.* at concentrations where the extracellularly facing K^+ sites are saturated. This Na^+ activation, therefore, reflects K^+ competition with Na^+ activation at the cytoplasm-facing sites, where the apparent Na^+ affinity is higher than the K^+ affinity (21, 22).

As seen in Fig. 4*A*, the data are well fit by the simplified model given by Scheme 1 and Equation 1. As $[K^+_{cyt}]$ is increased the curves are shifted progressively to the right, *i.e.* the intrinsic site dissociation constant for Na^+ increases with increasing inhibitor concentration, whereas the maximum activity is almost constant with the increasing K^+ concentration, as expected for pure competitive inhibition. A Dixon replot of $1/v$ *versus* inhibitor concentration, $[K^+]$, is also indicative of simple competitive inhibition with the intersection point of the lines above the $[K^+]$ axis at $1/v = 1/V_{max}$ (Fig. 4*B*). Indeed, Equation 2 is a simple and convenient tool to investigate the effects of pH on Na^+/K^+ selectivity. To that end, Na^+ activation curves were measured at pH values between 5.0 and 9.2, *i.e.* in the pH interval where the activity is stable. In Equation 2 the slope of the line, when the intrinsic Na^+ dissociation constant is plotted against K^+ concentration, represents the Na^+/K^+ selectivity, K^o_{Na}/K_K, where K^o_{Na} is the intercept on the y axis. Indeed, Na^+/K^+ selectivity can increase if the apparent Na^+ affinity ($1/K^o_{Na}$) decreases, or if the apparent K^+ affinity ($1/K_K$) increases, or both.

In Fig. 5 the intrinsic site dissociation constant for Na^+ calculated using Equation 1, assuming that both Na^+ and K^+ bind to the same E1 conformation at the cytoplasmic face and that the extracellularly facing sites are saturated with K^+ (19), is plotted against different fixed K^+ concentrations from 5 to 50 mM at pH values between 5.0 and 9.2. The data fit reasonably well to the straight-line Equation 2 with an intersection with the K'_{Na} axis at K^o_{Na} and a slope of K^o_{Na}/K_K. The simple model for evaluating the interaction of internal Na^+ and internal K^+ on the E1 enzyme intermediate therefore seems adequate under the experimental conditions used. As seen, the slopes of the plots are similar, and the intercepts increase with pH above 7.5 (Fig. 5*A*), whereas the opposite is true, *i.e.* the slopes

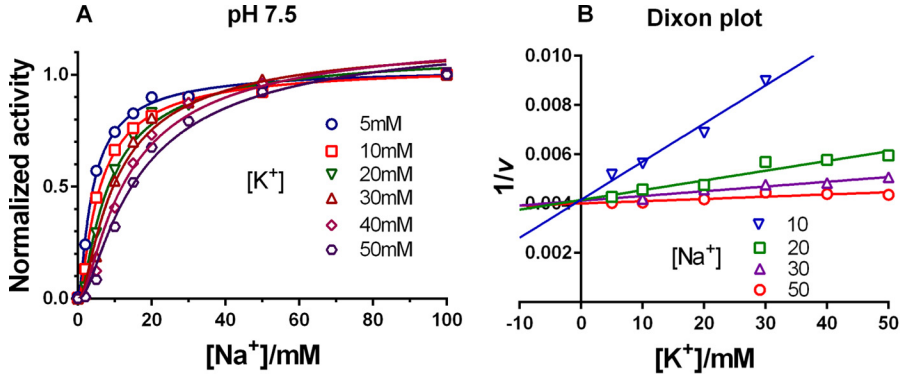

Figure 4. Na^+ activation of Na,K-ATPase activity at pH 7.5 at different fixed K^+ concentrations between 5 and 50 mM. *A*, the data are normalized (v/V_{max}) and are an average of three measurements with S.D. represented by the *error bars* (smaller here than the *symbols*). For each fixed K^+ concentration the enzyme activity is measured as a function of the Na^+ concentration. The curves are fit using Equation 1, taking $n_H = 3$ with K^+ competing at three cytoplasmic Na^+ sites. *B*, a Dixon plot with $1/v$ plotted against inhibitor concentration, [K^+] at different fixed substrate concentrations, [Na^+]. The intersection point is approximately at $1/V_{max}$.

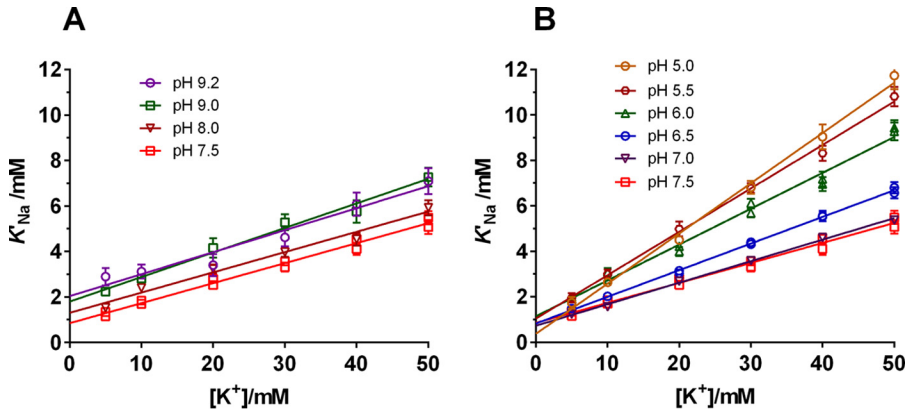

Figure 5. The intrinsic site dissociation constant for Na^+ evaluated using Equation 1 as a function of the fixed K^+ concentration at high pH values (*A*) and low pH values (*B*). The *lines* are computer-fit to the data using Equation 2, with no constraints on fit parameters.

increase and the intercepts are constant for pH values below 7.5 (Fig. 5*B*).

The dependence of the evaluated apparent ion-affinities and their ratio (selectivity = 1/slope) on pH is shown in Fig. 6. As indicated the apparent Na^+ affinity in the absence of K^+ ($1/K^0_{Na}$) is highest at pH ≤ 7.5, where it is almost constant at about 1 mM. However, at pH > 7.5, K^0_{Na} increases 2-fold to ~2 mM, *i.e.* the apparent Na^+ affinity in the absence of K^+ decreases with increasing pH. Almost the same pattern is observed regarding the apparent K^+ affinity ($1/K_K$), which means that the Na^+/K^+ selectivity (slope) only varies 2-fold over the pH range investigated. At a physiological pH of about 7.5, the slope is 0.088, *i.e.* the apparent cytoplasmic Na^+ affinity is about 11 times higher than the apparent K^+ affinity as a competitive inhibitor. This is the same value as was found in rat kidney enzyme by Therien and Blostein (2) using a similar experimental approach. As seen, the apparent affinities for Na^+ and K^+ increase very similarly at decreasing pH. The increase in slope observed at pH < 6.5 is due to a small preferential increase in apparent K^+ affinity over Na^+. Thus, at pH 5.0 the selectivity of the inward-facing binding sites for Na^+ over K^+ decreases about 5-fold (slope ~0.2).

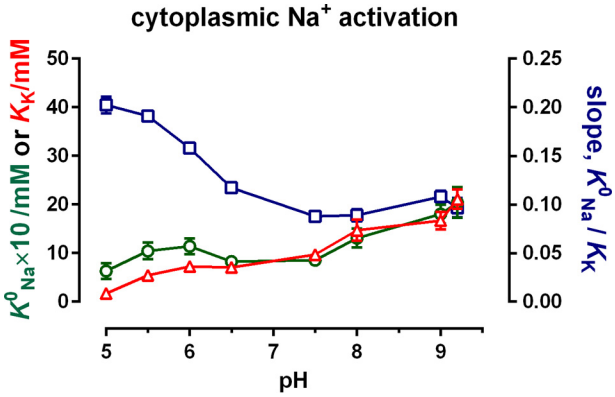

Figure 6. The apparent dissociation constant for Na^+ in the absence of K^+, $K^0_{Na} \times 10$ (○), and the apparent dissociation constant for K^+, K'_K (△), and their ratio (slope) (□) as deduced from the *y* and *x* intercepts and the slopes of the linear fit shown in Fig. 4.

Na^+/K^+ selectivity at the extracellular face of the Na,K-ATPase

Scheme 2 illustrates Na^+ competition for K^+ on the outward-facing sites to the E2P enzyme form (19). If Na^+ is assumed to be a simple competitive inhibitor at two extracellular K^+ sites, the K^+ activation curves at different fixed Na^+ concentrations can be described by Equation 3, derived from the steady-state solution of Scheme 2 (18, 19),

$$E2P \cdot K_2^+ \underset{k_{-K}}{\overset{k_K[K]^2}{\rightleftharpoons}} E2P \overset{k_{-Na}}{\underset{k_{Na}[Na]^2}{\rightleftharpoons}} E2P \cdot Na_2^+$$

Scheme 2

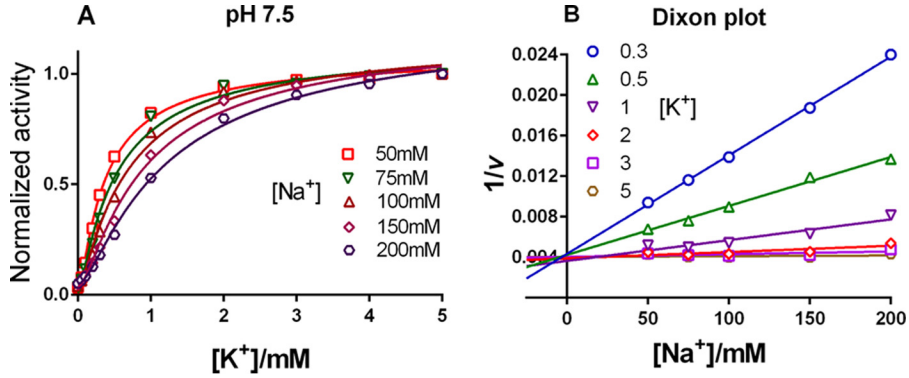

Figure 7. K^+ activation of Na,K-ATPase activity at pH 7.5 at different fixed Na^+ concentrations between 50 and 200 mM. *A*, the data are normalized (v/V_{max}) and are an average of three measurements with S.D. represented by the *error bars* (smaller than the *symbols*). For each fixed Na^+ concentration the enzyme activity is measured as a function of the K^+ concentration. The curves are fit using Equation 3, with Na^+ competing at two extracellular K^+ sites. *B*, Dixon plot with $1/v$ plotted against the inhibitor concentration, [Na^+], at different fixed substrate concentrations, [K^+]. The intersection point is approximately at $1/V_{max}$.

$$v = v_{min} + \frac{V_{max}}{(1 + K'_K/[K^+])^{n_H}} \quad \text{(Eq. 3)}$$

where K'_K is the intrinsic site dissociation constant for K^+,

$$K'_K = K^0_K + \frac{K^0_K}{K_{Na}}[Na^+_{ext}] \quad \text{(Eq. 4)}$$

As mentioned previously, the intrinsic site constant does not equal the half-saturation constant ($v = \frac{1}{2}V_{max}$ when $K_{0.5} = 2.4\ K'_K$ for $n_H = 2$, disregarding v_{min}). The term v_{min} is the activity in the absence of K^+ and corresponds to the Na^+-ATPase activity. At pH 7.2 the Na^+-ATPase activity amounts to 5% of V_{max} at 200 mM Na^+. Equation 4 is a straight-line relationship of K'_K *versus* the Na^+ concentration, where the *y* intercept is K^0_K, the apparent K^+ affinity without Na^+ present, and the slope is K^0_K/K_{Na}, a measure of the K^+/Na^+ selectivity. When the K^+ activation is investigated at various fixed Na^+ concentrations between 50 and 200 mM, where the cytoplasm-facing sites are near-saturated (*cf.* Fig. 4*A*), it reflects activation at the extracellularly facing ion sites, where the apparent K^+ affinity is higher than the Na^+ affinity (21, 22). In Fig. 7, K^+ activation curves are shown at pH 7.5 at various fixed Na^+ concentrations between 50 and 200 mM.

As seen from Fig. 7*A*, the model given by Scheme 2 and Equation 3 adequately describes the K^+ activation at various fixed Na^+ concentrations. As Na^+ is increased the curves are progressively shifted to the right, demonstrating an increasing intrinsic site dissociation constant for K^+ at increasing inhibitor concentration. The maximum activity is identical for all Na^+ concentrations larger or equal to 50 mM. At [Na^+] = 25 mM, V_{max} is reduced (by about 20%, not shown), demonstrating that 25 mM Na^+ is not saturating the cytoplasmic Na^+ sites, as also observed from Fig. 4. This inhibition pattern is as expected for pure competitive inhibition of K^+ activation by Na^+, as also indicated by the Dixon replot of $1/v$ *versus* the inhibitor concentration (Fig. 7*B*) with an intersection point approximately equal to $1/V_{max}$.

To investigate the effects of pH on Na^+/K^+ selectivity on the extracellularly facing binding sites, activation curves similar to the ones depicted in Fig. 7 were measured at pH values between 5.0 and 9.4. As seen for the Na^+ competition with extracellular K^+ at varying pH, the K^+ activation curves at both higher and lower pH are right-shifted at increasing Na^+ concentrations, indicating a lowering of the apparent K^+ affinity, whereas the maximum activity is almost constant with increasing Na^+ concentrations, as expected for pure competitive inhibition.

When the intrinsic site dissociation constant for K^+ (K'_K) given in Equation 4 is plotted against the fixed Na^+ concentrations at the various pH values, the data given in Fig. 8 result. As seen, the data appear to follow the expected straight-line relationships indicating that the simple model for evaluating the interaction of external K^+ and Na^+ on the E2 intermediate is adequate under the experimental conditions used.

The pH dependence of the Na^+/K^+ antagonism at the extracellularly exposed binding sites (Fig. 8) is very different from that observed at the cytoplasm-exposed sites (Fig. 5). The slopes decrease at pH values either below (Fig. 8*A*) or above (Fig. 8*B*) pH 7.5.

The results of an intercept/slope analysis are given in Fig. 9. The apparent dissociation constant for K^+ in the absence of Na^+ and the apparent dissociation constant for Na^+ have similar shapes except at pH values lower than about 6, where K_{Na} and K^0_K vary inversely with pH. At physiological pH, the extracellularly facing sites are about 400 times (1/slope) more selective for K^+ than for Na^+. The slope (K^0_K/K_{Na}) is at a minimum at low pH, where the K^+ selectivity over Na^+ reaches a value of 2.500. The selectivity of K^+ over Na^+ also increases at increasing pH values reaching 600 at pH 9.4. Thus, as also found for the cytoplasm-facing sites, K^+ selectivity over Na^+ increases at low pH. This change reflects a preferential increase in the apparent K^+ affinity over apparent Na^+ affinity.

pK_a estimations and protonation of key acidic residues

The differing ion affinities in the E1 and E2 states and their distinct variations with pH suggest that the stability of the individual ions in the binding sites varies between the two states. This stability must be determined by the detailed structure around the ion-binding sites, including the location of protons. It is conceivable that the locations of hydrogen ions change between different Na,K-ATPase conformations, which could

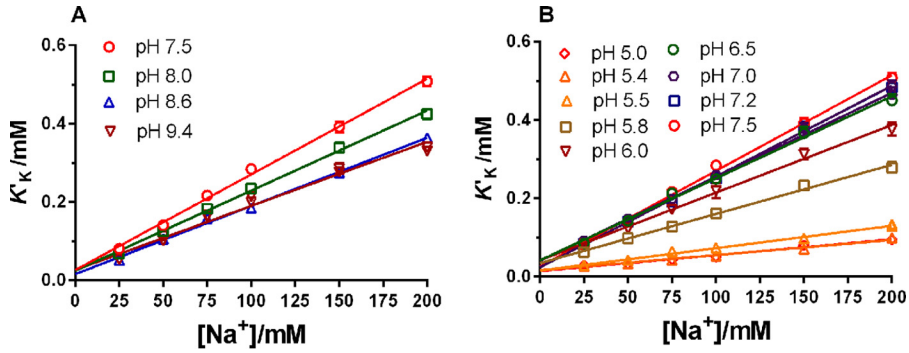

Figure 8. The intrinsic site dissociation constant for K^+ evaluated using Equation 3 as a function of the fixed Na^+ concentrations at various pH values. The lines are fit using Equation 4, with no constraints on fit parameters.

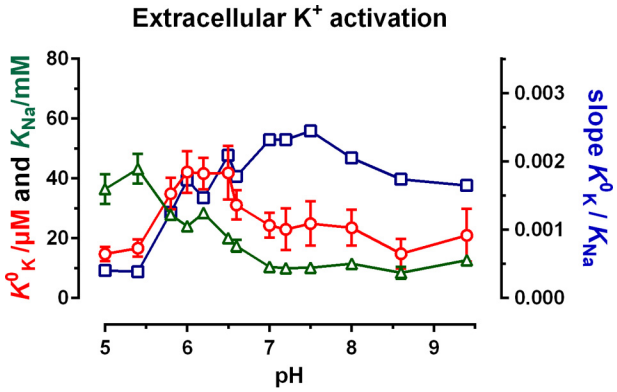

Figure 9. The apparent dissociation constant for K^+ in the absence of Na^+ (○), K^+/Na^+ selectivity, the slope (□), and the apparent dissociation constant for Na^+ (△) as deduced from the *y* and *x* intercepts and slope of the linear fit shown in Fig. 7.

include changes in the protonation states of acidic binding residues, as suggested from MD simulations of both E1 and E2 structures (13–15). The ion-binding sites of Na,K-ATPase are formed by four TM helices (Fig. 1, M4, M5, M6, and M8). These TM helices contribute six key acidic residues (Glu^{327}, Glu^{779}, Glu^{954}, Asp^{804}, Asp^{808}, and Asp^{926}), all of which are implicated in Na^+/K^+ selectivity (13–15). The K^+-coordinating acidic residues comprise Glu^{327} of M4 (Glu^{334} in shark), Glu^{779} of M5 (Glu^{786}), and Asp^{804} of M6 (Asp^{811}). Asp808 of M6 (Asp^{815}) is included, although it does not directly coordinate a K^+ ion, but it stabilizes a K^+-coordinating water molecule (16). Two of the Na^+-binding sites share the same four residues, Glu^{327}, Glu^{779}, Asp^{804}, and Asp^{808}, which coordinate Na^+ at sites I and II, whereas the Na^+-specific site III also includes Asp^{926} of M8, although its interaction with Na^+ at site III is marginal (distance 4.2 Å). However, it is conceivable that site III initially binds Na^+ closer to Asp^{926}, as indicated by its slightly different location in the two protomers in the crystals, see below (3). Glu^{954} may participate, as it is implicated in a putative "C-terminal ion pathway" as postulated from neurological disease mutations (23, 24), although the N-terminal pathway for Na^+ entry is more likely under physiological conditions according to the high-resolution Na^+-bound structure (3).

Although the location of the hydrogen molecules has not yet been determined experimentally, protonation states can be gauged by estimating the empirical pK_a values in both the E1 and E2 states. Table 1 shows the pK_a values as estimated by PROPKA 3.1 (25) compared with values estimated by multi-conformation continuum electrostatic calculations (MCCE) (26); they accommodate van der Waals and electrostatic energies differently and do not explicitly incorporate hydrogen bonding. Atomic models based on the crystal structures of Na,K-ATPase in the E2·Pi·$2K^+$ state (PDB ID: 2ZXE) and E1~P·ADP·$3Na^+$ state (PDB ID: 3WGV and 3WGU) were used in the calculations. The estimated values must be regarded as tentative for several reasons. First, as seen from Fig. 10, the available crystal structures represent enzyme conformations that succeed the conformational states that actually bind the Na^+ (E1·ATP) and K^+ ions (E2-P). Thus, there may be structural rearrangements of side chains of acidic residues in the actual ion-binding conformations that are not accommodated in the calculations. Indeed, even small structural variations occurring in the two protomers in the 3WGU structures (protomers A and C) result in reversed pK_a values for Glu^{327} and Asp^{804} calculated by PROPKA 3.1 (10.9 and 5.3, respectively, for protomer A, but 6.1 and 10.6 for protomer C), a situation also apparent when comparing the two structures, 3WGV and 4HQJ (*cf.* Ref. 14). Furthermore, the pK_a values calculated by PROPKA and MCCE may be interdependent, due to coupling of coordinating residues in the cation-binding sites. This is especially important in regard to Glu^{327}, Glu^{779}, and Asp^{804}, all of which are strongly coupled in the crystal structures of the two main structures, and in addition, in regard to Asp^{808} in the E1 state (Table 1 and Fig 11). Finally, the parameter value for the dielectric constant (ϵ) of the protein interior is uncertain. Normally, a value of 4 is chosen for larger proteins.

As seen in Table 1, in the K^+-binding E2 conformation, represented by the E2·Pi·$2K^+$ structure, the pK_a values estimated by both PROPKA and MCCE indicate that at physiological pH 7.5 the three Glu residues and Asp^{926} are protonated, whereas Asp^{804} and Asp^{808} are deprotonated. The protonation of Glu^{327}:Oϵ2 and Glu^{779}:Oϵ1 is in accord with the crystal structure of the E2·Pi·$2K^+$ state (16), where the distances between the carboxylates of these two residues and the carbonyl of Val^{325} and Asp^{804}:Oδ2 are only 3.0 and 2.8 Å, respectively (Fig. 12).

In the Na^+-binding E1 conformation represented by the E1~P·ADP·$3Na^+$ structure, Glu^{954} is protonated, and Asp^{808} and Asp^{926} are deprotonated according to MCCE and PROPKA. The protonation states of Glu^{327}, Glu^{779}, and Asp^{804} are more ambiguous, as mentioned above, and individual pK_a values assigned by MCCE seem particularly unreliable. Instead,

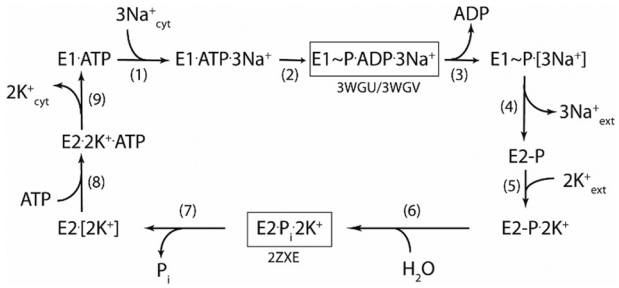

Figure 10. The reaction cycle of Na,K-ATPase with the two high-resolution crystal structures *framed*.

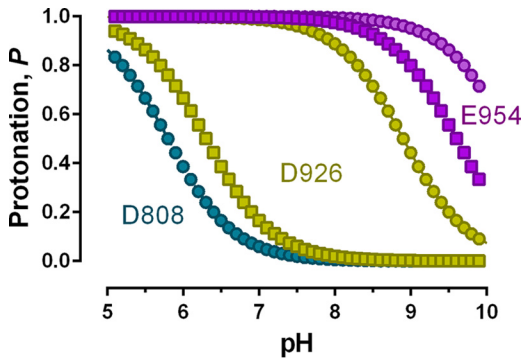

Figure 11. Protonation of acidic residues that are not strongly coupled in the K^+- and Na^+-binding sites as a function of pH using the pK_a values calculated by PROPKA 3.1 (Table 1) and the Henderson-Hasselbalch equation. ■, E1 state; ●, E2 state.

with MCCE, we treated the three residues as a group as described below under "Experimental procedures." The distance between Glu^{327}:Oϵ2 and Asp^{804}:Oδ2 is only 2.8 Å in the E1~P·ADP·$3Na^+$ crystal structure, implying that at least one of these residues (probably Glu^{327} according to PROPKA (Table 1)) is protonated (Fig. 11). The protonation state of Glu^{779}:Oϵ2 is more uncertain. Thus, although the distance between Glu^{779}:Oϵ1 and Ser^{775}:O in 3WGV(A) is short (2.8 Å), the geometry is irregular for a hydrogen bond, and further, Ser^{775}:O makes a hydrogen bond with Glu^{779}:N. As there are two other polar oxygen atoms, Asp^{804}:Oδ1 and Asp^{808}:Oδ1, near Glu^{779}:Oϵ1, this region may be short of protons. Thus Glu^{779}:Oϵ2 could be protonated rather than Asp^{804}:Oδ1 and Asp^{808}:Oδ1. If Glu^{779}:Oϵ2 is protonated, the hydrogen bond may be bifurcated.

The protonation states of the acidic residues at different pH values can in principle be calculated using the Henderson-Hasselbalch (H-H) equation,

$$P = \frac{1}{1 + 10^{\mathrm{pH}-\mathrm{p}K_a}} \qquad \text{(Eq. 5)}$$

where P is the protonation probability. However, the H-H equation may not apply to residues that are strongly coupled, like Glu^{327}, Glu^{779}, Asp^{804}, and Asp^{808} in the E1 state and Glu^{327}, Glu^{779}, and Asp_{804} in E2. The protonation probabilities of conformers at various pH values were also estimated by MCCE using Monte-Carlo simulations. This yielded pH-dependent protonation probabilities for each ionizable residue. Using the pK_a values calculated by PROPKA for the noncoupled residues given in Table 1, the protonation profiles of these binding residues in the E2 and E1 states at pH values between 5.0 and 10.0 are shown in Fig. 11. As seen, the most pronounced difference between the K^+- and the Na^+-binding conformations is a left-shift of the curve for Asp^{926}. There is a slight right-shift of the protonation curves for Glu^{954}. In the E2 state a decrease of pH from the physiological value of 7.5 to 5.0 predicts an increase in the protonation probability of Asp^{808}. On the other hand, Glu^{954} and Asp^{926} have an increased probability to ionize on increasing the pH from 7.5 to 10.0 (Fig. 11). The protonation probabilities calculated using MCCE in the E2 state appear to follow the H-H equation and indicate the following order of proton affinities: $Glu^{779} > Glu^{954} > Asp^{926} > Glu^{327} > Asp^{808} > Asp^{804}$); the same order is obtained using the PROPKA results. Within the range of pH 5 to 10, four carboxylate groups are protonated. Asp^{808}, which coordinates K^+ site I, appears to become protonated only below pH 5, whereas Glu^{327} near site II ionizes above pH 10.

In the E1 state the pK_a values for Asp^{808} and Glu^{954} indicate that they are deprotonated and protonated, respectively, at physiological pH. Asp^{926} appears to become protonated only at values below physiological pH. The pH profiles for Glu^{327}, Glu^{779}, and Asp^{804} do not conform to the H-H equation, in agreement with their strong coupling. The order of proton affinities in the E1 state is: $Glu^{954} > Glu^{779} > Asp^{804} > Glu^{327} > Asp^{926} > Asp^{808}$. It seems that the group of residues comprising Glu^{327}, Glu^{779}, and Asp^{804} acquires a proton as pH is decreased and loses a proton as it is increased.

Discussion

The pH dependence of Na,K-ATPase activity is characterized by a bell-shaped curve about the physiological pH optimum of 7.5 (Fig. 2). The decline in activity on either side of the optimum is reversible between pH 5 and 9.4 and irreversible outside of these limits (Fig. 2). The reversible inhibition must result from the formation of new inhibitory ionic forms and the irreversible inactivation from the loss of structural integrity, as demonstrated by increased trypsin sensitivity (Fig. 3).

We determined the Na^+/K^+ selectivity at the cytoplasm-facing and extracellularly facing ion-binding sites independently using a model of simple competition between Na^+ and K^+ at three cytoplasmic Na^+ sites on E1 and two extracellular K^+ sites on E2, in accordance with studies on the Na,K-ATPase in red cells (18, 19, 27–30). The linear relationships of K'_{Na} *versus* $[K^+]$ in Fig. 5 and of K'_K *versus* $[Na^+]$ in Fig. 8 are strong indications that the simplified model in which Na^+ and K^+ bind randomly to the same enzyme intermediate (E1 and E2, respectively) is adequate under the experimental conditions used. Indeed, we found that the apparent ion affinity decreased as the inhibitor/competing ion concentration increased, and V_{max} remained unchanged (*cf.* Figs. 4 and 7) (31). Crucially, in this system, the ion affinities could be investigated independently at the two faces of the pump by separating them functionally, because of their different apparent Na^+ and K^+ affinities.

Our major finding was to demonstrate the distinct sidedness of pH effects on apparent ion affinities and Na^+/K^+ selectivity as summarized in Figs. 6 and 9. The Na^+ sites are selective for Na^+ over K^+ by a factor of about 11 (1/slope) at pH ≥ 7.5, and half that at lower pH. The latter is due to a slight increase in K^+ affinity (70% change) and a decrease in that of Na^+ (22%). An

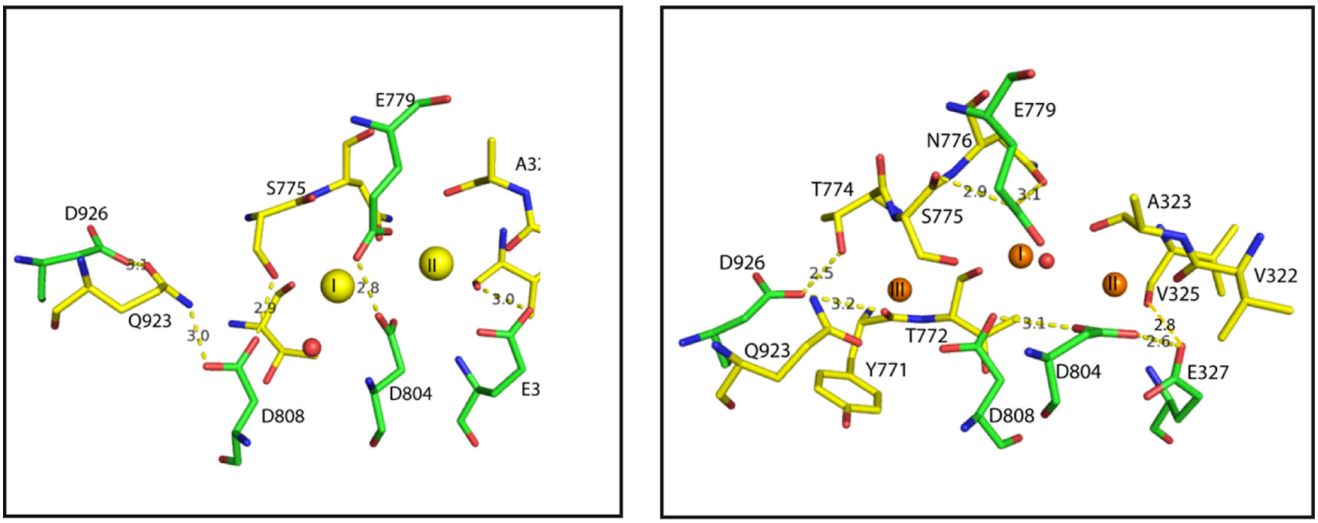

Figure 12. Distance between coordinating residues around the K^+ ion-binding site (*left*, PDB ID 2ZXE) and the Na^+ ion-binding sites (*right*, PDB ID 3WGV, protomer A). Critical distances (Å) to carboxylate oxygens of key acidic residues (*green sticks*) are shown.

alkaline pH slightly lowers Na^+ selectivity over K^+ due to lowered Na^+ affinity, but the effect is small, and the affinities for Na^+ and K^+ change almost proportionately with pH.

For the outward-facing K^+ sites, a lowering of pH is associated with a dramatic increase in selectivity for K^+ over Na^+, from a factor of about 400 at physiological pH to about 2500 at pH 5 (Fig. 9). Slope analysis reveals that this is due to an increase in the apparent K^+ affinity and a decrease for Na^+. Increasing pH from 7.5 to 9.4 also increases selectivity for K^+, but less profoundly, from 400- to 600-fold (Fig. 9).

Recent high-resolution crystal structures of Na,K-ATPase in the K^+ bound E2·P state (16) and the Na^+-bound E1~P·ADP state (3) suggest that Na^+/K^+ selectivity at the two faces of the pump is critically dependent on the detailed structure of the ion-binding sites and that size discrimination is an important feature. On the cytoplasmic side, the Na^+ sites are constrained and tightly juxtaposed so as to accommodate smaller ions. On the extracellular side, the K^+-binding sites are looser to accommodate larger ions, as the spread of coordinating atoms can only weakly interact with small ions.

Several coordinating residues are common to both sites, as shown in Table 1 and Fig. 1. Glu^{327}, Glu^{779}, and Asp^{804} coordinate both the K^+ and Na^+ ions. Asp^{808} coordinates both Na^+ sites I and III and indirectly coordinates K^+ site I through an intervening water molecule (16). In addition, Asp^{926} is important for apparent Na^+ affinity (24) and is involved indirectly as an ion-coordinating residue through a hydrogen bond with Thr^{774}:Oγ1, which coordinates Na^+ site III in the E1~P·ADP·3Na^+ state (3). Protonation of Glu^{327}, Glu^{779}, and Asp^{808} is required to establish the strong selectivity for K^+ over Na^+ at sites I and II of the E2·Pi·2K^+ state (13), as is the case for the corresponding residues in the E2 state of SERCA1a (32). Rui *et al.* (14) have hypothesized from MD simulations using the high-resolution structure 3WGV (3) that a different set of residues is protonated in E1 compared with E2, where the protonation states of aspartates 808 and 926 are reversed between the two conformations.

For the inward-facing Na^+ sites, our pK_a calculations suggest that the modest change in Na^+/K^+ selectivity at low pH may be caused by protonation of Asp^{926}, which is close to Na^+ at site III (Figs. 11 and 12). It is uncertain whether the protonation state of Asp^{804} also changes, as the estimated pK_a value is unreliable due to strong coupling to Glu^{327}, Asp^{808}, and Glu^{779}. Asp^{926} is 4.2 Å from Na^+ site III and seemingly only marginally involved in Na^+ coordination. However, as mentioned previously it is possible that Na^+ initially binds more closely to Asp^{926} in the E1ATP state, as occurs in protomer A in the E1~P·ADP·3Na^+ crystals (3). Furthermore, Asp^{926} is involved in an extensive hydrogen-bonding network, which includes Tyr^{774} and Gln^{854}, to stabilize the Na^+-binding sites (3). This seems to be in accord with the free energy perturbation calculations done by Rui *et al.* (14) demonstrating that the charge neutralizing the D926N mutation eliminates Na^+ selectivity. In fact, D926N mutants have a decreased apparent Na^+ affinity, despite a slight E1/E2 conformational shift toward E1 (33). For the outward-facing K^+ sites, pK_a estimations suggest that increasing pH results in deprotonation of Asp^{926} and perhaps Glu^{327}. The latter is uncertain because of the ambiguous pK_a calculation caused by the strong coupling to Glu^{779} and Asp^{804}. However, mutation of Glu^{327} to a Gln removes the inhibition of hydrolytic activity observed at high pH, compatible with ionization of this residue at alkaline pH in the wild type (17). Lowering the pH from 7.5 to 5.0, which has such a profound effect on selectivity, appears mainly to protonate Asp^{808}, as it has an estimated pK_a value of 5.8 (PROPKA analysis, Table 1). Protonation of both Glu^{327}, which coordinates K^+ site II, and Asp^{808}, which is indirectly involved in the coordination of K^+ site I, may be very important for establishing the physiological selectivity of K^+ over Na^+ at the K^+ sites. Paradoxically, the K^+ over Na^+ selectivity is lowest at physiological pH.

The protonation state of Asp^{926} in the binding sites of Na,K-ATPase under physiological conditions is different in E1 (deprotonated) and E2 (protonated), whereas Asp^{808} is deprotonated in both states according to the pK_a values estimated from PROPKA and MCCE (Table 1). The different protonation state of Asp^{926} is in accordance with the results of Rui *et al.* (14). Free-energy calculations by all-atom MD, which explicitly incorporate hydrogen atom interactions, resulted in pK_a values

for Asp^{804} in the E1 state of 9.2 (14) and for Asp^{808} in the E2 state of 9.4, respectively (13), *i.e.* both are protonated in the respective states at pH 7.5. Indeed, Asp^{808}:Oδ2 is only 2.9Å from Ser^{775}:Oγ in the E2 state, and Asp^{804}:Oδ2 is only 2.6 Å from Glu^{327}:Oϵ2 in the E1 state; these are close distances that favor protonation (Fig. 12). The dynamic protonation/deprotonation reactions of Asp^{926} have been suggested to be integral to the overall Na,K-ATPase reaction and to the different Na^+ and K^+ selectivities associated with the E1/E2 states, and proton exchange between cation sites and the cytoplasm at physiological pH has been postulated previously (26), ideas that are reinforced by our findings (*cf.* Refs. 34 and 35). On a cautionary note, the pK_a values calculated by MD simulations may be questionable because of the empirical force field employed (CHARMM) (36) not dealing with hydrogen bonding realistically. It is, therefore, unclear whether the thermodynamically averaged structure obtained by MD simulations is the same as that derived from X-ray analysis, which is important because small structural differences could significantly influence estimated pK_a values. Furthermore, both the charge and conformation of the side chains of the coordinating residues are critical, as demonstrated recently for the charge selectivity of ligand-gated ion channels (37).

In conclusion, the distinct difference in Na^+/K^+ selectivity at the two faces of Na,K-ATPase as a function of pH, where outward-facing K^+ sites become increasingly selective for K^+ below and above pH 7.5 due to a preferential increase in K^+ affinity over Na^+ and the inward-facing Na^+ sites exhibit decreased selectivity for Na^+ over K^+ at low pH due to preferential increased affinity for K^+, changing hardly at all at high pH, may be a consequence of the changes in ionization state of key acidic ion-binding residues. Our pK_a calculations suggested that Asp^{804}, Asp^{808}, and Asp^{926} ionize between pH 4.5 and 9.5, and other residues may as well, but electrostatic coupling prevents making firm conclusions here. Outside of this pH range irreversible inactivation occurs. Ionization or protonation of ion-coordinating residues may be another mechanism, besides the size of binding sites, for controlling cation selectivity. This may be important in the kidney nephron, where large variations in pH and ionic conditions occur. It also may help to counteract hyperkalemia under acid conditions (38).

Finally, although such changes in residues coordinating the cations seem likely to be involved in the pH and selectivity changes, it cannot be excluded that the effects are indirect through, for example, changes in the E1/E2 equilibrium or local structural changes around the exposed ion-binding sites.

Experimental procedures

Preparation of Na,K-ATPase

Na,K ATPase from the outer medulla of pig kidney was prepared according to the method of Jørgensen (39) using SDS extraction followed by differential centrifugation to isolate Na,K-ATPase enriched membrane fragments.

Measurement of Na,K-ATPase activity

The specific enzyme activity was measured using the method of Baginski *et al.* (40). The optimum hydrolytic activity was measured at 23 °C in a test medium that contained 130 mM NaCl, 20 mM KCl, 4 mM $MgCl_2$, 3 mM ATP, and 20 mM buffer depending on pH. The optimum specific activity was ~2100 $\mu mol \cdot mg^{-1} \cdot h^{-1}$ at 37 °C under standard conditions as described by Ottolenghi (41). In analyzing the Na^+/K^+ selectivity, enzyme activity was measured at saturating concentrations of one of the ions, Na^+ or K^+, while the concentration of the other was varied. Thus, in measuring Na^+/K^+ selectivity at the cytoplasm-facing binding sites, the activity was measured at increasing Na^+ concentrations and at a fixed K^+ concentration of 5, 10, 20, 30, 40, or 50 mM, which are all saturating at the extracellularly facing binding sites. Similarly, in analyzing Na^+/K^+ selectivity at the extracellular facing binding sites, the activity was measured at increasing K^+ concentrations and at a fixed Na^+ concentration of 50, 75, 100, 150, or 200 mM, which is saturating for the cytoplasm-facing binding sites. The variation in ionic strength was without effect on the activation curves, as controlled by experiments where choline chloride was used to keep the ionic strength constant (not shown). The protein content was determined by the method of Lowry *et al.* (42) as modified by Peterson (43) using bovine serum albumin as the standard.

Trypsin digestion

Trypsin cleavage of Na,K-ATPase after preincubation at different pH values was performed as described previously (44). Briefly, protein was suspended in a buffer containing 30 mM histidine, imidazole, or MES, depending on the actual pH, 150 mM NaCl (E1) or KCl (E2), and 20 mM $MgCl_2$. The protein was preincubated for 45 min at 24 °C before the addition of 0.3 $\mu g/\mu l$ trypsin after adjusting the pH to 7.4. Proteolysis was allowed to proceed for 45 min at 24 °C followed by quenching with SDS sample buffer containing 0.5% TCA.

Gel electrophoresis and immunoblotting

Protein fragments were separated using SDS-PAGE (3% stacking gel, 8% resolving gel). Between 7 and 15 μg of protein was loaded to each lane. The gels were stained by Coomassie Blue or transferred onto PVFD membranes for immunostaining using a semidry blotter. Following a 2-h transfer, the membranes were washed twice with phosphate-buffered saline and incubated with primary antibody (α1002–1016, kindly provided by J. V. Møller) overnight at room temperature. The membranes were washed as described previously and incubated with secondary goat anti-rabbit antibody for 2 h at room temperature. Proteins were visualized by treatment with ECL reagent (Amersham Biosciences) according to the manufacturer's procedure.

Digital imaging

Analyses of SDS-gels and immunoblots were performed using ImageQuant TL software (Amersham Biosciences).

Numerical analysis of pK_a

The protonation state of six key acidic residues in the binding sites for extracellular K^+ and cytoplasmic Na^+, respectively, was evaluated using the Poisson-Boltzmann equation, employing MCCE (version 2.7 in the full mode) (26) and using atomic models based on the crystal structures of Na,K-ATPase in the

$E2{\cdot}Pi{\cdot}2K^+$ state (PDB ID: 2ZXE) (16) and $E1{\sim}P{\cdot}ADP{\cdot}3Na^+$ state (PDB ID: 3WGV and 3WGU) (3). The target system derived from the crystal structures included 400 amino acid residues, ions, and water molecules in the membrane region. In the calculations for the E2 state (2ZXE), the system was composed of residues Ile^{90}-Gln^{150}, Thr^{282}-Ala^{352}, and Ala^{756}-Tyr^{1023} plus the two K^+ ions and the 39 water molecules in the membrane region. The system used for the E1 state (3WGV and 3WGU) includes residues Val^{83}-Gln^{143}, Thr^{275}-Ala^{345}, and Ala^{749}-Tyr^{1016} plus the three Na^+ ions and the five water molecules in the membrane. Different values of the protein dielectric constant between 4 and 16 were used to assess sensitivity to this parameter in the MCCE calculations. Empirical pK_a values were also estimated using PROPKA 3.1 (25). We calculated the probabilities of protonation states for the six key acidic residues of Na,K-ATPase by MCCE. Their pH dependences indicate that three residues, Glu^{327}, Glu^{779}, and Asp^{804}, are strongly coupled in the E1 state. Similar coupling is also indicated by PROPKA. Coupling is expected by geometrical analyses of the crystal structures, because the carboxyl group of Asp^{804} is close to those of Glu^{327} and Glu^{779}. Thus, it is difficult to determine each pK_a value independently. However, this interdependency also indicates that the proton affinities of the three residues must be similar. Treating all three residues together, we plotted the sum of the probabilities of the protonation as a function of pH and treated it as composed of three Henderson-Hasselbalch equations with three parameters, pK_{a1}, pK_{a2}, and pK_{a3}. The plots indicated that one of the three parameters must be larger than 14.0; the other two parameters were determined by Excel Solver.

Statistical analysis and modeling

Results are expressed as mean ± S.D., and $p < 0.05$ is regarded as significant in all comparisons. The program Prism 6 was used to analyze the data. Structural models were prepared using PyMOL.

Author contributions—F. C. conceptualization; F. C. formal analysis; F. C. and N. T. investigation; F. C. writing-original draft; F. C., N. T., and C. T. writing-review and editing.

Acknowledgments—We thank Anette Damsgaard and Hanne Kidmose for excellent technical assistance. We are grateful to D. B. McIntosh for help in improving the manuscript.

References

1. Kaplan, J. H. (2002) Biochemistry of Na,K-ATPase. *Annu. Rev. Biochem.* **71,** 511–535 CrossRef Medline
2. Therien, A. G., and Blostein, R. (1999) K^+/Na^+ antagonism at cytoplasmic sites of the Na^+-K^+-ATPase: A tissue-specific mechanism of sodium pump regulation. *Am. J. Physiol. Cell Physiol.* **277,** C891–C898 CrossRef Medline
3. Kanai, R., Ogawa, H., Vilsen, B., Cornelius, F., and Toyoshima, C. (2013) Crystal structure of a Na^+-bound Na^+,K^+-ATPase preceding the E1P state. *Nature* **502,** 201–206 CrossRef Medline
4. Breitwieser, G. E., Altamirano, A. A., and Russell, J. M. (1987) Effects of pH on sodium pump fluxes in squid giant axons. *Am. J. Physiol. Cell Physiol.* **253,** C547–C554 CrossRef Medline
5. Salonikidis, P. S., Kirichenko, S. N., Tatjanenko, L. V., Schwarz, W., and Vasilets, L. A. (2000) Extracellular pH modulates kinetics of the Na^+,K^+-ATPase. *Biochim. Biophys. Acta* **1509,** 496–504 CrossRef Medline
6. Milanick, M. A., and Arnett, K. L. (2002) Extracellular protons regulate the extracellular cation selectivity of the sodium pump. *J. Gen. Physiol.* **120,** 497–508 CrossRef Medline
7. Skou, J. C. (1979) Effects of ATP on the intermediary steps of the reaction of the (Na^+ + K^+)-ATPase. IV. Effect of ATP on $K_{0.5}$ for Na^+ and on hydrolysis at different pH and temperature. *Biochim. Biophys. Acta* **567,** 421–435 CrossRef Medline
8. Skou, J. C., and Esmann, M. (1980) Effects of ATP and protons on the Na:K selectivity of the (Na^+ + K^+)-ATPase studied by ligand effects on intrinsic and extrinsic fluorescence. *Biochim. Biophys. Acta* **601,** 386–402 CrossRef Medline
9. Sugita, Y., Miyashita, N., Ikeguchi, M., Kidera, A., and Toyoshima, C. (2005) Protonation of the acidic residues in the transmembrane cation-binding sites of the Ca^{2+} pump. *J. Am. Chem. Soc.* **127,** 6150–6151 CrossRef Medline
10. Toyoshima, C. (2008) Structural role of countertransport revealed in Ca^{2+} pump crystal structure in the absence of Ca^{2+}. *Arch. Biochem. Biophys.* **476,** 3–11 CrossRef Medline
11. Musgaard, M., Thøgersen, L., and Schiøtt, B. (2011) Protonation state of important acidic residues in the central ion binding sites of the Ca^{2+}-ATPase: A molecular modeling study. *Biochemistry* **50,** 11109–11120 CrossRef Medline
12. Lervik, A., Bresme, F., and Kjelstrup, S. (2012) Molecular dynamics simulation of the Ca^{2+}-pump: A structural analysis. *Phys. Chem. Chem. Phys.* **14,** 3543–3553 CrossRef Medline
13. Yu, H., Ratheal, I. M., Artigas, P., and Roux, B. (2011) Protonation of key acidic residues is critical for the K^+-selectivity of the Na/K pump. *Nat. Struct. Mol. Biol.* **18,** 1159–1163 CrossRef Medline
14. Rui, H., Artigas, P., and Roux, B. (2016) The selectivity of the Na^+/K^+-pump is controlled by binding site protonation and self-correcting occlusion. *eLIFE* **5,** e16616 Medline
15. Han, M., Kopec, W., Solov'yov, I. A., and Khandelia, H. (2016) Glutamate water gates in the ion binding pocket of Na^+ bound Na^+,K^+-ATPase. *Sci. Rep.* **7,** 39829–39838 Medline
16. Shinoda, T., Ogawa, H., Cornelius, F., and Toyoshima, C. (2009) Crystal structure of the sodium-potassium pump at 2.4 Å resolution. *Nature* **459,** 446–451 CrossRef Medline
17. Vilsen, B. (1993) Glutamate 329 located in the fourth transmembrane segment of the α-subunit of the rat kidney Na^+,K^+-ATPase is not an essential residue for active transport of sodium and potassium ions. *Biochemistry* **32,** 13340–13349 CrossRef Medline
18. Garay, R. P., and Garrahan, P. J. (1973) The interaction of sodium and potassium with the sodium pump in red cells. *J. Physiol.* (*Lond.*) **462,** 297–325
19. Sachs, J. R. (1986) The order of addition of sodium and release of potassium at the inside of the sodium pump of the human red cell. *J. Physiol.* **381,** 149–168 CrossRef Medline
20. Peluffo, R. D., González-Lebrero, R. M., Kaufman, S. B., Kortagere, S., Orban, B., Rossi, R. C., and Berlin, J. R. (2009) Quaternary benzyltriethylammonium ion binding to the Na,K-ATPase: A tool to investigate extracellular K^+ binding reactions. *Biochemistry* **48,** 8105–8119 CrossRef Medline
21. Simons, T. J. (1974) Potassium: potassium exchange catalysed by the sodium pump in human red cells. *J. Physiol.* **237,** 123–155 CrossRef Medline
22. Skou, J. C. (1974) The (Na^+ + K^+)-activated enzyme system and its relationship to transport of sodium and potassium. *Q. Rev. Biophys.* **7,** 401–434 Medline
23. Poulsen, H., Khandelia, H., Morth, J. P., Bublitz, M., Mouritsen, O. G., Egebjerg, J., and Nissen, P. (2010) Neurological disease mutations compromise a C-terminal ion pathway in the Na^+/K^+-ATPase. *Nature* **467,** 99–102 CrossRef Medline
24. Einholm, A. P., Toustrup-Jensen, M. S., Holm, R., Andersen, J. P., and Vilsen, B. (2010) The rapid-onset dystonia parkinsonism mutation D923N of the Na^+, K^+-ATPase α3 isoform disrupts Na^+ interaction at the third Na^+ site. *J. Biol. Chem.* **285,** 26245–26254 CrossRef Medline

25. Bas, D. C., Rogers, D. M., and Jensen, J. H. (2008) Very fast prediction and rationalization of pK_a values for protein-ligand complexes. *Proteins* **73,** 765–783 CrossRef Medline
26. Song, Y., Mao, J., and Gunner, M. R. (2009) MCCE2: Improving protein pK_a calculations with extensive side chain rotamer sampling. *J. Comput. Chem.* **20,** 2231–2247
27. Glynn, I. M. (1962). Activation of adenosinetriphosphatase activity in a cell membrane by external potassium and internal sodium. *J. Physiol.* **160,** 18P–19P
28. Sen, A. K., and Post, R. L. (1964) Stoichiometry and localization of adenosinetriphosphate-dependent sodium and potassium transport in the erythrocyte. *J. Biol. Chem.* **239,** 345–352 Medline
29. Whittam, R., and Ager, M. (1965) The connection between active cation transport and metabolism in erythrocytes. *Biochem. J.* **97,** 214–227 CrossRef Medline
30. Garrahan, P. J., and Glynn, I. M. (1967) The stoichiometry of the sodium pump. *J. Physiol.* **192,** 217–235 CrossRef Medline
31. Cleland, W. W. (1963) The kinetics of enzyme-catalyzed reactions with two or more substrates or products. I. Nomenclature and rate equations. *Biochim. Biophys. Acta* **67,** 104–137 CrossRef Medline
32. Obara, K., Miyashita, N., Xu, C., Toyoshima, I., Sugita, Y., Inesi, G., and Toyoshima, C. (2005) Structural role of countertransport revealed in Ca^{2+} pump crystal structure in the absence of Ca^{2+}. *Proc. Natl. Acad. Sci. U.S.A.*, **102,** 14489–14496
33. Holm, R., Einholm, A. P., Andersen, J. P., and Vilsen, B. (2015) Rescue of Na^+ affinity in aspartate 928 mutants of Na^+,K^+-ATPase by secondary mutation of glutamate 314. *J. Biol. Chem.* **290,** 9801–9811 CrossRef Medline
34. Vedovato, N., and Gadsby, D. (2014) Route, mechanism, and implications of proton import during Na^+/K^+ exchange by native Na^+/K^+-ATPase pumps. *J. Gen. Physiol.* **143,** 449–464 CrossRef Medline
35. Koenderink, J. B., Geibel, S., Grabsch, E., De Pont J. J. H. H. M, Bamberg, E., and Friedrich, T. (2003) Electrophysiological analysis of the mutated Na,K-ATPase cation binding pocket. *J. Biol. Chem.* **278,** 51213–51222 CrossRef Medline
36. Brooks, B. R., Brooks C. L., 3rd, Mackerell, A. D., Jr., Nilsson, L., Petrella, R. J., Roux, B., Won, Y., Archontis, G., Bartels, C., Boresch, S., Caflisch, A., Caves, L., Cui, Q., Dinner, A. R., Feig, *et al.* (2009) CHARMM: The biomolecular simulation program. *J. Comput. Chem.* **30,** 1545–1614 CrossRef Medline
37. Cymes, G. D., and Grossman, C. (2016) Identifying the elusive link between amino acid sequence and charge selectivity in pentameric ligand-gated ion channels. *Proc. Natl. Acad. Sci. U.S.A.* **113,** E7106–E7115 CrossRef
38. Terkildsen, J. R., Crampin, E. J., and Smith, N. P. (2007) The balance between inactivation and activation of the Na^+-K^+ pump underlies the triphasic accumulation of extracellular K^+ during myocardial ischemia. *Am. J. Physiol. Heart Circ. Physiol.* **293,** H3036–H3045 CrossRef Medline
39. Jørgensen, P. L. (1974) Purification and characterization of ($Na^+ + K^+$)-ATPase. III. Purification from the outer medulla of mammalian kidney after selective removal of membrane components by SDS. *Biochim. Biophys. Acta*, **356,** 36–52
40. Baginski, E. S., Foa, P. P., and Zak, B. (1967) Determination of phosphate: Study of labile organic phosphate interference. *Clin. Chim. Acta* **14,** 155–158
41. Ottolenghi, P. (1975) The reversible delipidation of a solubilized sodium-plus-potassium ion-dependent adenosine triphosphatase from the salt gland of the spiny dogfish. *Biochem. J.* **151,** 61–66 CrossRef Medline
42. Lowry, O. H., Rosebrough, N. J., Farr, A. L., and Randall, R. J. (1951) Protein measurement with the folin phenol reagent. *J. Biol. Chem.* **193,** 265–275 Medline
43. Peterson, G. L. (1977). A simplification of the protein assay method of Lowry *et al.* which is more generally applicable. *Anal. Biochem.* **83,** 346–356
44. Mahmmoud, Y. A., and Cornelius, F. (2002) Protein kinase C phosphorylation of purified Na,K-ATPase: C-terminal phosphorylation sites at the α- and γ-subunits close to the inner face of the plasma membrane. *Biophys. J.* **82,** 1907–1919 CrossRef Medline